DYRK1A Interacts with the Tuberous Sclerosis Complex and Promotes mTORC1 Activity

Pinhua Wang[1†], Sunayana Sarkar[2†], Menghuan Zhang[1†], Tingting Xiao[1], Fenhua Kong[1], Zhe Zhang[1], Deepa Balasubramanian[2], Nandan Jayaram[6], Sayantan Datta[2‡], Ruyu He[1], Ping Wu[3], Peng Chao[3], Ying Zhang[4], Michael P. Washburn[4,5], Laurence Florens[4], Sonal Nagarkar-Jaiswal[6], Manish Jaiswal[2*], Man Mohan[1,7*]

Affiliations

1 State Key Laboratory of Primate Biomedical Research, Institute of Primate Translational Medicine, Kunming University of Science and Technology, Kunming, China.

2 Tata Institute of Fundamental Research, Hyderabad, 500046, India.

3 National Facility for Protein Science in Shanghai, Zhangjiang Lab, Shanghai, 201210, China.

4 Stowers Institute for Medical Research, 1000 East 50th Street, Kansas City, Missouri 64110, USA.

5 Department of Cancer Biology, The University of Kansas Medical Center, 3901 Rainbow Boulevard, Kansas City, Kansas 66160, USA.

6 CSIR–Centre for Cellular and Molecular Biology, Habsiguda, Uppal Road Hyderabad, 500007, India.

7 Department of Biochemistry and Molecular Cell Biology, Shanghai Key Laboratory of Tumor Microenvironment and Inflammation, Shanghai Jiaotong University School of Medicine, Shanghai 200025, China.

† These authors contributed equally to this work

‡ Current address: Centre for Writing and Pedagogy, School of Interwoven Arts and Sciences, Krea University, Sri City, AP, 517647, India

E-mail: manmohan2100@outlook.com, manish@tifrh.res.in

Keywords: Microcephaly, Cell growth, Minibrain, Drosophila, Neuromuscular Junction

Abstract

DYRK1A, a ubiquitously expressed kinase, is linked to the dominant intellectual developmental disorder, microcephaly and Down syndrome in humans. It regulates numerous cellular processes such as cell cycle, vesicle trafficking and microtubule assembly. DYRK1A is a critical regulator of organ growth; however, how it regulates organ growth is not fully understood. Here, we show that the knockdown of *DYRK1A* results in reduced cell size, which depends on mTORC1. Using proteomic approaches, we found that DYRK1A interacts with the Tuberous sclerosis complex (TSC) proteins, namely TSC1 and TSC2, which negatively regulate mTORC1 activation. Further, we show that DYRK1A phosphorylates TSC2 at T1462, a modification known to inhibit TSC activity and promote mTORC1 activity. We also found that the reduced cell growth upon knockdown of DYRK1A can be rescued by overexpression of RHEB, an activator of mTORC1. Our findings suggest that DYRK1A inhibits TSC complex activity through inhibitory phosphorylation on TSC2, thereby promoting mTORC1 activity. Further, using the *Drosophila* neuromuscular junction as a model, we show that the *mnb*, the fly homologues of *DYRK1A*, is rescued by RHEB overexpression, suggesting a conserved role of *DYRK1A* in TORC1 regulation.

1. Introduction

The *Dual-Specificity Tyrosine Phosphorylation-Regulated Kinase 1A (DYRK1A)* is a ubiquitously expressed kinase that belongs to the CMGC group (Cyclin-dependent kinases, Mitogen-activated protein kinase, Glycogen synthase kinases and CDK-like kinases group). *DYRK1A,* is located within the Down syndrome Critical Region (DSCR). The phenotypes associated with Down syndrome (1), including abnormal neurodevelopment (2, 3), and increased susceptibility to acute megakaryoblastic leukaemia (4), have been reasoned to be due to an increased expression of *DYRK1A*. On the other hand, haploinsufficiency of *DYRK1A* causes DYRK1A syndrome, a rare autosomal dominant disease characterized by intellectual disability, intrauterine growth retardation, microcephaly and stunted growth (5-7). Mouse models heterozygous for *Dyrk1a* also show a reduction in brain and body size (8, 9). In *Drosophila*, loss of *mnb*, the *Drosophila* homolog of DYRK1A, results in reduced organ size, including brain, legs and wings (10, 11). Therefore, *DYRK1A* is a critical regulator of organ growth (12); however, the cellular processes by which *DYRK1A* promote organ growth are unclear.

DYRK1A and its homologs have also been implicated in many cellular processes, such as cell cycle, signal transduction, gene expression, vesicle trafficking and microtubule assembly (13). DYRK1A has been shown to extend the G1 phase of the cell cycle in neuroblastoma cells by phosphorylation and subsequent degradation of cyclin D1 (14). In glioblastoma cells, DYRK1A phosphorylates ubiquitin ligase CDC23, which mediates mitotic protein degradation, thereby promoting tumor growth (15). Further, DYRK1A expression positively correlates with EGFR levels, and DYRK1A inhibitors reduce EGFR-dependent glioblastoma growth (16). DYRK1A promotes the expression of several genes required for ribosomal biogenesis and protein translation (17, 18); for example, RPS6 ribosomal protein S6, a component of the 40S subunit, and translation initiation factor, EIF4A3 (19). However, if the regulation of these genes by DYRK1A is physiologically significant, it is currently unknown.

The Mechanistic Target of Rapamycin Complex 1 (mTORC1) is a key energy sensor and a master regulator of anabolic processes (20). The mTORC1 promotes anabolic processes such as protein, nucleotide and lipid synthesis and represses catabolic processes such as autophagy, thereby promoting cellular growth (21, 22). The mechanism of mTORC1-mediated regulation of multiple anabolic pathways has been studied extensively (20-22). The Tuberous Sclerosis Complex (TSC), consisting of TSC1, TSC2 and TBC1D7 (TBC1 domain family member 7),

integrates various extracellular signals and negatively regulates mTORC1 complex activity (20, 23). TSC2 is a GTPase-activating protein (GAP) and promotes the conversion of GTP-bound RHEB (Ras Homolog Enriched in Brain) to the GDP-bound state, thereby inhibiting it. When TSC2 is inhibited, the GTP-bound RHEB activates mTORC1 (24, 25). The mTORC1 activation is controlled by extracellular stimuli, nutrients, energy status, and stress. For example, in response to insulin stimulation, AKT phosphorylates TSC2 at several sites, including S939 and T1462, suppressing its inhibitory effect on RHEB-GTP recycling, thus activating mTORC1 (26). Similarly, in response to growth factors, Extracellular signal-Regulated Kinase (ERK) (27) and p90 Ribosomal S6 Kinase 1 (RSK1) phosphorylate TSC2 and activate mTORC1 (28). MK2 (MAP kinase-activated protein kinase 2/ MAPKAPK2) phosphorylates TSC2 at yet another site, S1210, in the presence of serum and leads to the inhibition of TSC2 activity, which allows the activation of mTORC1 (24). Catabolic signals, such as low energy levels during glucose scarcity, drive AMPK-mediated phosphorylation of TSC2 that promotes its GAP function and suppresses mTORC1 activity (29). Several kinases regulating the TSC activity underscores the importance of investigating novel kinases involved in its regulation, which may regulate mTORC1 activity in distinct cellular contexts.

In this study, we discover that DYRK1A interacts with TSC1 and TSC2. We show that DYRK1A phosphorylates TSC2 at T1462 and is a possible positive regulator of mTORC1 activity and cell growth. Further, we show that in *Drosophila*, both Mnb, the DYRK1A-homolog, and mTORC1 are required to promote Neuromuscular Junction (NMJ) growth. Moreover, the activation of mTORC1 can rescue the NMJ growth phenotype of *mnb* loss of function, suggesting Mnb may regulate mTORC1 to promote neuromuscular junction morphology. We propose that DYRK1A-mediated regulation of mTORC1 activity is a conserved mechanism to regulate cell size and development.

2. Results

2.1 DYRK1A promotes cell growth

To study the function of *DYRK1A*, we knocked down DYRK1A in multiple cell lines, including in HEK293 cells (18). We noticed that DYRK1A-depleted cells were smaller than the control cells. To explore if DYRK1A has a role in maintaining cell size, we performed a systematic analysis of the cell size phenotypes after transient knockdown of *DYRK1A* in HEK293 and observed a reduction in cell size (**Figure 1A-B**). Since mutations in *DYRK1A*

are associated with stunted growth and microcephaly, we wondered if neuronal cells require *DYRK1A* to maintain proper cell size. Therefore, we knocked down *DYRK1A* in the human neuroblastoma cell line SH-SY5Y and observed a significant reduction in cell size (Figure 1 C-D). Further, we tested if the observed cell size phenotype is conserved in mice. We targeted *Dyrk1a* in NIH-3T3 using CRISPR/Cas9 and observed a significant reduction in cell size (Figure 1E-F). Our data suggests that *DYRK1A* promotes cell size across cell lines derived from different models and tissues. Thus, we tested if the overexpression of *DYRK1A* can promote cell size. Since strong overexpression of *DYRK1A* leads to cell cycle exit (2, 30, 31), we used the Doxycycline-inducible system to express low levels of *Flag-DYRK1A* in HEK293 cells (32). We noted a change in cell size with an increasing dosage of Doxycycline, which reached a saturation state at 100ng/ml Doxycycline in our system (**Supplementary figure 1**). We observed a significant increase in cell size at 40 ng/ml Doxycycline treatment for 48 hours when the *DYRK1A* mRNA levels were approximately twice that of control (Figure 1G-H). At this level of *DYRK1A* mRNA expression, overexpressed Flag-DYRK1A was undetectable by western blot. Overall, our knockdown and overexpression experiments in different cell lines, including both human and mouse, suggest that *DYRK1A* promotes cell size.

2.2 DYRK1A physically interacts with the Tuberous Sclerosis Complex

To understand how *DYRK1A* promotes cell growth, we investigated DYRK1A protein-interactors. Previously, we have identified protein-interactors of wild-type and kinase-dead DYRK1A (K188R) from HEK293 cells using affinity purification and mass spectrometry (18, 32). In these purifications, we have observed significant enrichment of DCAF7, ARIP4, RB1, EP300, CREBBP, TRAF2, TRAF3, FAM53C, RNF169, many of which have also been identified by many other groups as bona-fide DYRK1A interacting proteins (33-37). We also observed significant enrichment of TSC components TSC1 and TSC2 among proteins co-purified with wild-type and kinase-dead DYRK1A (K188R) (**Figure 2A**). Interestingly, a few peptides of TBC1D7, the third component of TSC, were also detected in the wild-type pull-down (see dNSAF values in Figure 2 A), suggesting that DYRK1A interacts with the TSC complex. This interaction is intriguing as TSC is a negative regulator of the mTORC1, which is known to promote cell growth (38-40).

To ascertain the interaction between DYRK1A and TSC, we expressed *Flag-DYRK1A* in HEK293 cells through the Doxycycline-inducible system and performed Flag affinity purification. Surprisingly, when we used HEPES buffer containing either 0.5% NP40 or 1%

Tween 20, we did not detect co-purification of TSC2 with Flag-DYRK1A (data not shown). However, when we prepared extracts by lysing the cells in hypotonic buffer without detergent followed by Dounce homogenization, we found that both TSC1 and TSC2 co-purify with Flag-DYRK1A (Figure 2B). Further, we tested the interaction between endogenous DYRK1A and TSC by immunoprecipitating DYKR1A; we observed co-purification of both TSC1 and TSC2 (Figure 2C). Immuno-affinity purification of overexpressed HA3-TSC1 and Flag-TSC2 was also able to pull down endogenous DYRK1A (Supplementary Figure 2). These results confirmed that DYRK1A physically interacts with the TSC complex. We then sought to identify the domains of DYRK1A that interact with TSC1, as TSC1 is the scaffolding protein in the TSC (20). We co-overexpressed HA3-TSC1 and various truncated forms of Flag-DYRK1A in HEK293 cells (**Supplementary Figure 3**). We found that interaction between DYRK1A and TSC1 was abolished in all the truncated forms that lack DYRK1A kinase domain, which suggests that DYRK1A kinase domain is required for the interaction (**Supplementary Figure 3**). We further confirmed that DYRK1A interacts with TSC1 through its kinase domain by co-expressing the FLAG-tagged DYRK1A kinase domain and HA3-TSC1, followed by immunoprecipitation using anti-FLAG antibodies (Figure 2D). Taken together, our results show that DYRK1A physically interacts with the TSC.

2.3 DYRK1A promotes mTORC1 activity

Next, we sought to test the implications of TSC and DYRK1A interaction on mTORC1 activity. mTORC1 is known to be induced in HEK293 cells by treatment with fetal bovine serum (FBS), insulin, and many growth factors following serum starvation (21, 22, 41, 42). We performed similar experiments, where we knocked down *DYRK1A* followed by serum starvation and tested for levels of pS6K, a reporter for mTOR activity. We did not observe a significant reduction in basal phosphorylation levels on S6K and S6. However, 10 and 20 min after FBS treatment, we observed significantly reduced levels of Phospho-S6K and Phospho-S6 in *DYRK1A* KD compared to control HEK293 cells (Figure 3A-C). Further, we tested the levels of pS6K and pS6 in NIH3T3 after CRISPR-mediated targeting of *Dyrk1a*. Interestingly, we found significant reductions in pS6K and pS6 compared to controls (Figure 3 D-F). Overall, our results indicate that DYRK1A is required to promote mTORC1 activity.

2.4 DYRK1A phosphorylates TSC2 at T1462

Next, we investigated if DYRK1A phosphorylates TSC1/TSC2, which is known to regulate mTORC1 activity. For this, we first knocked down *DYRK1A* in HEK293 cells, co-expressed

HA3-TSC1 and *Flag-TSC2* and performed immunoprecipitation followed by LC/tandem MS (MS/MS) to identify the phosphorylation status of TSC1 and TSC2 in these cells. We observed that *DYRK1A* knockdown samples have reduced TSC2 phosphorylation at T1462 (T1462) compared to the control samples. T1462 has been previously identified as a site phosphorylated by various kinases that activate the mTORC1 pathway, including AKT (26), ERK (27), p90 ribosomal S6 kinase 1 (RSK1) (28), IκB kinase β (IKKβ) (43), and MAPKAPK2 (MK2) (24) in response to insulin and other growth factors. To ascertain that indeed, TSC2 T1462 is the site phosphorylated by DYRK1A, we performed *in-vitro* kinase assays using purified wild-type and kinase-dead DYRK1A. As TSC2 is about 200KDa protein, we purified transiently overexpressed HA3-TSC1 and Flag-TSC2 from HEK293 cells and performed *in vitro* kinase assay on beads. Wild-type DYRK1A autophosphorylates and runs as fuzzy bands around 90-100Kda in polyacrylamide gels, whereas kinase-dead DYRK1A runs only as a single sharp band (Figure 4A). In our assay, we did not observe an increase in phosphorylation at S1387 or Serine 939 in the presence of ATP and DYRK1A (Figure 4A). However, immunopurified TSC2 is heavily phosphorylated at Serine 1387 and Serine 939, which are two important sites that are phosphorylated by AKT(26, 41, 43). Therefore, we cannot rule out if the immunopurified TSC2 was fully phosphorylated at S1387 and S939. However, it is important to note that we did not observe any differential loss of phosphorylation in TSC2 at S1387 in our mass spectrometry phosphorylation analysis. Interestingly, we found T1462 was strongly phosphorylated by wild-type DYRK1A, not by kinase-dead DYRK1A (Figure 4A). Taken together, these experiments demonstrate that DYRK1A phosphorylates TSC2 on T1462. This phosphorylation is known to be an inhibitory modification and it is a key site that gets phosphorylated by various other key regulators of the mTORC1 pathway (43). We could not perform in-vitro tests to check if DYRK1A phosphorylates TSC1 or other sites on TSC2 due to the lack of appropriate antibodies. The overall data suggest that DYRK1A mediates TSC2 T1462 phosphorylation to inhibit TSC activity, promoting TORC1 activity.

2.5 RHEB overexpression can rescue cell growth phenotype of *DYRK1A* knockdown

TSC phosphorylation has been shown to inhibit TSC, and activate mTORC1 via RHEB, where the activation of TSC leads to the hydrolysis of GTP-bound RHEB, which in turn leads to mTORC1 inhibition (20). We hypothesized that DYRK1A-mediated phosphorylation of TSC2 may promote mTORC1 activation in a RHEB-mediated manner. Therefore, we reasoned that overexpression of *RHEB* will rescue the cell size phenotype caused by *DYRK1A*

knockdown. We overexpressed *RHEB* in *DYRK1A* knockdown cells and found a partial rescue of cell size, suggesting that DYRK1A indeed plays a role in cell size regulation at least partly upstream to RHEB (Figure 4B and C). Further, inhibition of mTOR with either Rapamycin or Torin1 rescued the increased cell size phenotype mediated by overexpression of *DYRK1A* in the inducible HEK293A-Flag-DYRK1A model (Supplementary Figure 4). These data suggest that DYRK1A phosphorylates TSC2, which inhibits its action, leading to the activation of mTORC1 via RHEB.

2.6 *Drosophila mnb* mutants show reduced neuromuscular junctions, which can be rescued by RHEB overexpression

Since the TSC-TOR pathway is conserved in *Drosophila* (44), we sought to test if the DYRK1A-mediated regulation of the TSC-TOR pathway is also conserved. The TOR pathway is shown to promote neuromuscular junction (NMJ) development in flies (45, 46) (Figure 5B, G). Similarly, *mnb*, the fly homolog of DYRK1A, is also required for NMJ growth (47); however, the mechanism of *mnb*-mediated NMJ growth is unknown. Based on our finding that *DYRK1A* promotes TOR activity, we hypothesized that *mnb* promotes larval NMJ growth through TOR. To test this hypothesis, we systematically compared the NMJ growth phenotype of *mnb* mutant with that of loss or gain of TOR activity at larval NMJ. Since TOR mutants are early larval lethal, we expressed dominant-negative TOR (*TOR.Ted*) in motor neurons using the UAS-Gal4 system (*D42Gal4>UAS-TOR.Ted*) (48). To activate the TOR pathway, we overexpressed *RHEB* in motor neurons (*D42Gal4>UAS-RHEB*) (49). We stained NMJ using anti-HRP (to mark neurons) and anti-DLG (to mark boutons where synaptic connections are formed). As shown in Figure 5 (A, B, G), the loss of *mnb* causes a reduction in the NMJ bouton numbers compared to the wild-type control (WT, Canton S)—similarly, the expression of TOR.TED in motor neurons (*D42Gal4>UAS-Tor.Ted*) also causes a reduction in NMJ bouton numbers (Supplementary Figure S5 D-F). In contrast, overexpression of *mnb* in motor neurons increases the bouton numbers (Figure 4 C, D, H). Similarly, the activation of the TOR pathway by overexpression of *RHEB* in motor neurons or mutations in *gigas* (*gig*, the fly homolog of *TSC2*) increases the number of boutons (Fig 5 E, F, I, Supplementary Figure S5 C). The similarities in the TOR and *mnb* phenotypes suggest that Mnb may positively regulate TOR activity and promote NMJ growth. To test this hypothesis, we asked whether or not the NMJ phenotype of the *mnb* mutant is rescued by the activation of TOR. As shown in Figure 5L, overexpression of *RHEB* rescues the NMJ bouton numbers in *mnb* mutants. These results indicate that *RHEB* functions downstream to *mnb* to

regulate the NMJ development. Taken together, the results in mammalian cells and flies suggest that the role of DYRK1A/Mnb in regulating the TOR pathway is conserved.

3 Discussion

This work shows that DYRK1A promotes cell size as a reduction in *DYRK1A* levels in both human and mouse cells results in small cell size (Figure 1A-D). mTORC1 is a key energy sensor and a master regulator of cell growth (21, 22). We found that reduced levels of *DYRK1A* in cells result in decreased S6K and S6 phosphorylation, suggesting that DYRK1A positively regulates mTORC1 (Figure 3). One of the key regulators of mTORC1 is the TSC complex, consisting of TSC1, TSC2 and TBC1D7 (TBC1 domain family member 7), which integrates various extracellular signals and negatively regulates mTORC1 complex activity (20, 23). DYRK1A physically interacts with TSC complex through its kinase domain (Figure 2). TSC2 is a GTPase-activating protein (GAP) that promotes the conversion of GTP-bound RHEB to the GDP-bound state, thereby inhibiting it. When TSC2 is inhibited, the GTP-bound RHEB activates mTORC1 (25, 41). Phosphorylation at TSC2 at T1462 has been shown to inhibit TSC and promote TORC1 activity through RHEB (43, 50). Our study, for the first time, shows that DYRK1A phosphorylates TSC2 at the T1462 site, thereby promoting the mTORC1 pathway. We also show that the overexpression of *RHEB* could partially rescue the cell growth phenotypes exhibited by *DYRK1A* knockdown cells, indicating that the DYRK1A works upstream to RHEB.

In DYRK1A syndrome, loss of one copy of *DYRK1A l*eads to stunted growth and microcephaly in humans (7)**.** A recent report showing a reduction in mTOR signaling in mice cortex lacking *Dyrk1a* indicates that the DYRK1A-mTORC1 axis may regulate brain development (51). In *Drosophila*, *mnb* is widely expressed in the developing central nervous system and has been linked to post-differentiation roles in neurons. For example, in flies, *mnb* has been linked to long-term memory formation (52). In humans and mice, *DYRK1A* has been linked to the neurite spine morphogenesis, and it has been suggested that the neurite spine phenotype may contribute to intellectual disability in Down syndrome (53-55). The phenomenon of NMJ morphogenesis in fruit flies is analogous to neurite spine morphogenesis. The TOR pathway is shown to promote neuromuscular junction (NMJ) development in flies (45, 46) (Figure 5B, G). Similarly, *mnb* is also required for NMJ growth (47); however, the mechanism of *mnb*-mediated NMJ growth was unknown. Our results show that the reduction in NMJ size in *mnb* mutants can be rescued by *RHEB* overexpression,

suggesting that Mnb positively regulates mTORC1. Our results are also supported by a study in *Arabidopsis* that showed YAK1, a DYRK kinase, regulates meristem activity through the mTOR pathway (56). Overall, our results suggest that the role of Mnb/DYRK1A in the regulation of mTORC1 pathway is evolutionarily conserved, and the DYRK1A-mTORC1 axis plays a crucial role in neuronal morphogenesis and cellular growth.

Figure 1. DYRK1A regulates cell size.

shRNA-mediated knockdown of *DYRK1A* was performed in **(A-B)** HEK293 and **(C-D)** SH-SY5Y cells using lentivirus. Transduced cells were selected for four days before analysis. Western blot shows the efficiency of *DYRK1A* knockdown. **(E-F)** NIH3T3 cells were treated with *Dyrk1a*-targeting sgRNA expressing lentivirus and selected for four days before analysis. Western blot shows the efficiency of *DYRK1A* knockdown. **(G-H)** HEK293 cells expressing *Flag-DYRK1A* and the parental cells were treated with 40ng/ml Doxycycline for 48 hours and analyzed for cell size. (G) Overexpression was analyzed by qRT-PCR. GAPDH mRNA was used to normalize RNA in q-RT-PCR samples. Data represent the mean ± SD (n = 3 biological replicates).

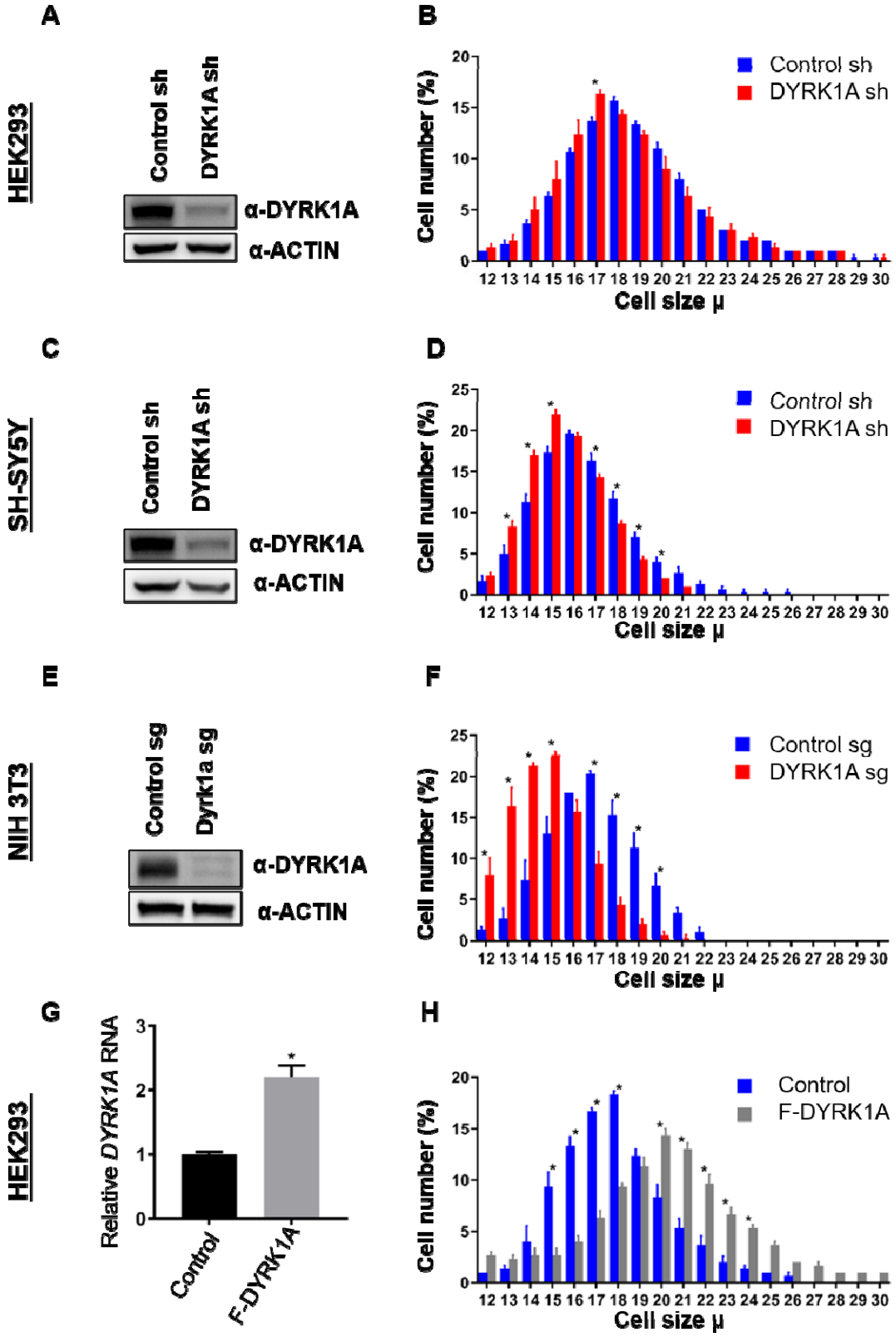
A
HEK293
Control sh
DYRK1A sh
α-DYRK1A
α-ACTIN
B
Control sh
DYRK1A sh
Cell number (%)
Cell size µ
C
SH-SY5Y
Control sh
DYRK1A sh
α-DYRK1A
α-ACTIN
D
Control sh
DYRK1A sh
Cell number (%)
Cell size µ
E
NIH 3T3
Control sg
Dyrk1a sg
α-DYRK1A
α-ACTIN
F
Control sg
DYRK1A sg
Cell number (%)
Cell size µ
G
HEK293
Relative DYRK1A RNA
Control
F-DYRK1A
H
Control
F-DYRK1A
Cell number (%)
Cell size µ

Figure 2. DYRK1A interacts with the Tuberous Sclerosis Complex

(A) The MS/MS datasets previously acquired by MudPIT analyses of FLAG-DYRK1A affinity purifications and negative FLAG controls (18) were searched against the most recent releases of the human protein sequence databases (built by collating and removing redundant entries from NCBI *Homo sapiens* RefSeq GCF_000001405.40_GRCh38.p14 and GCF_009914755.1_T2T-CHM13v2.0). Highly enriched proteins include known and novel DYRK1A-interacting partners and are reported with their peptide counts and distributed Normalized Spectral Abundance Factor (dNSAF) values, which reflect their relative abundance in the samples (57). **(B)** Flag beads were used to pull-down Flag-DYRK1A from whole cell extracts of HEK293 transfected with Flag-DYRK1A, Protein A beads were used as a control. The blots were probed with TSC1 and TSC2 antibodies. Actin was used to normalize the lysates inputs. **(C)** endogenous DYRK1A was immunoprecipitated with DYRK1A antibody from HEK293 cytoplasmic fraction generated using the Dignam protocol (18) and probed with antibodies against endogenous DYRK1A, TSC1 and TSC2. Rabbit IgG was used as the IP control **(D)** Flag-DYRK1A and Flag-DYRK1A kinase domain constructs were affinity purified using Flag-beads from HEK293 cells co-transfected with HA3-TSC1 and probed with α-HA and α-Flag antibodies. Actin was used as the loading control.

A DYRK1A Protein Interactions

	FLAG-DYRK1A		FLAG-DYRK1A-KD		FLAG-Control (x2)
Proteins	Peptides	dNSAF	Peptides	dNSAF	Peptides
DYRK1A	39	0.0174	35	0.0472	0
DCAF7	27	0.1925	23	0.1850	0
ARIP4	43	0.0033	20	0.0020	0
RB1	14	0.0020	18	0.0075	0
EP300	26	0.0009	31	0.0038	0
CREBBP	23	0.0004	34	0.0012	0
TRAF2	15	0.0056	13	0.0055	0
TRAF3	6	0.0008	12	0.0049	0
FAM53C	14	0.0137	11	0.0107	0
RNF169	7	0.0011	1	0.0002	0
TSC1	11	0.0007	23	0.0039	0
TSC2	6	0.0002	33	0.0048	0
TBC1D7	2	0.0005	0	0	0

B

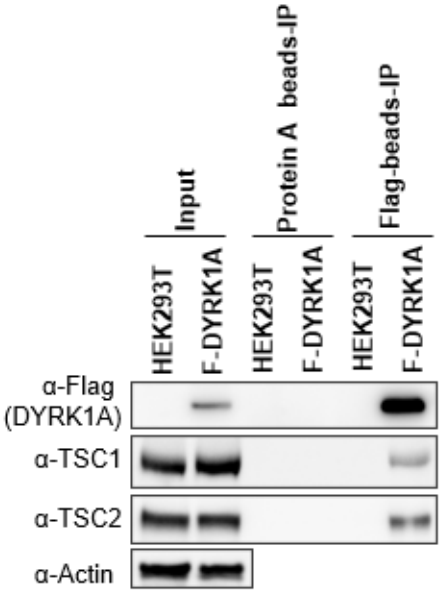

C

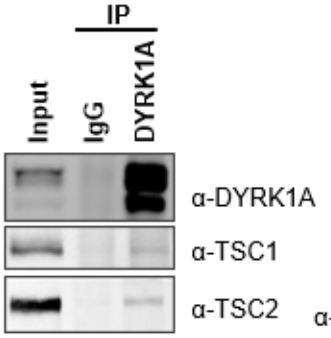

D

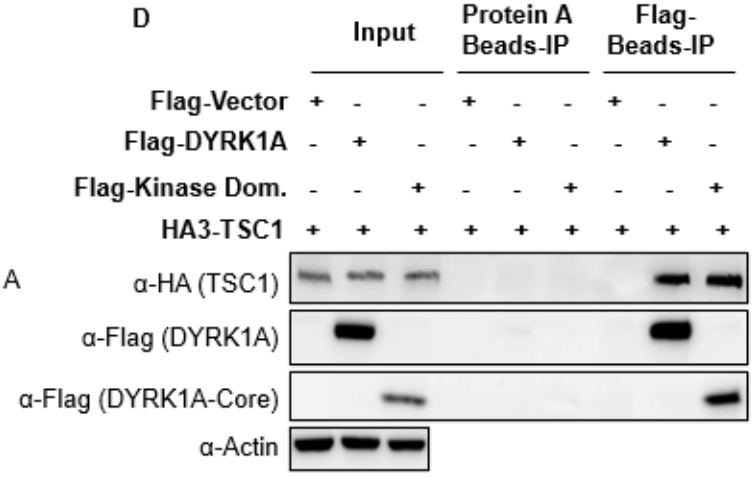

Figure 3. DYRK1A promotes the activation of mTORC1 pathway in human and mouse cells. (A) HEK293 cells treated with *DYRK1A* shRNA or control shRNA were serum starved for 12 hours before being activated with serum for the indicated times. Cells were then harvested, lysates and probed with the indicated antibodies. Actin was used as the loading control.

(B - C) Quantification of proteins in A, levels of pS6K (T389), S6K, pS6 (pS235/236) and S6 were quantified using Image J software and the ratio of pS6K/S6K and pS6/S6 were plotted (n = 3 biological replicates). **(D)** NIH3T3 cells were treated with sgRNA-targeting *Dyrk1a* or non-targeting control and selected for four days with Puromycin before harvesting. Lysates were probed with indicated antibodies. **(E - F)** Quantification of proteins in D**,** levels of pS6K (T389), S6K, pS6 (pS235/236) and S6 were quantified (as described for B and C) and ratios were plotted (n = 3 biological replicates). Student's *t* tests were done to compare samples. *p* value = * ($p < 0.05$).

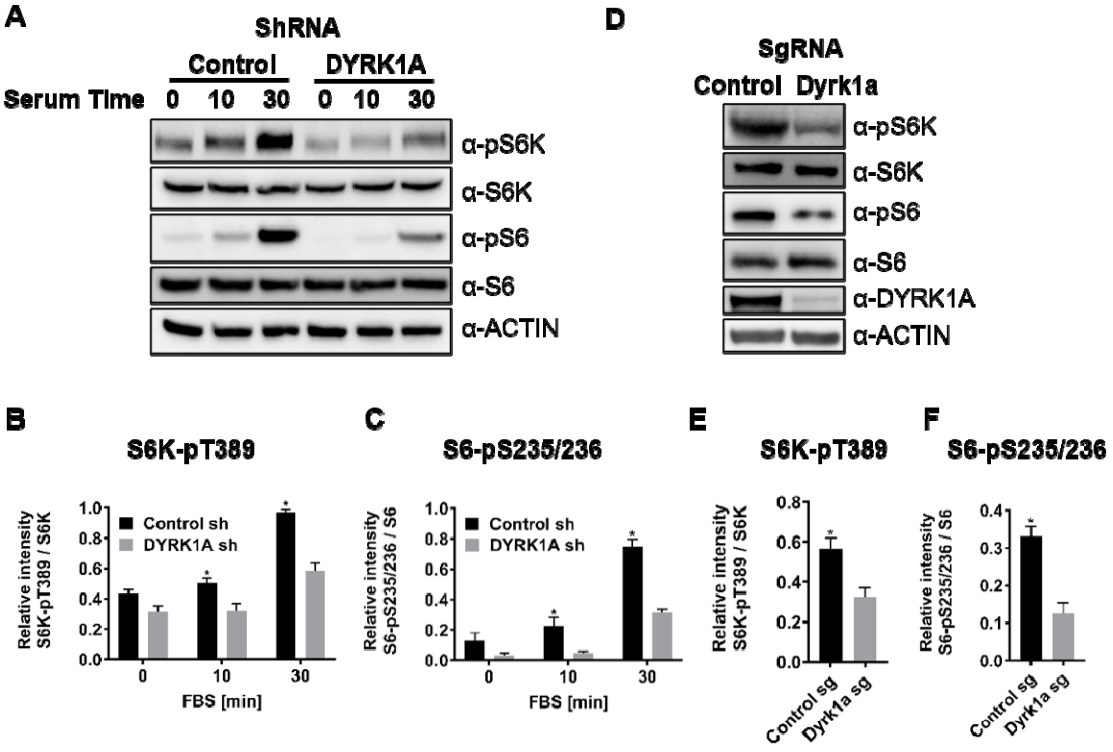

Figure 4. DYRK1A phosphorylates TSC2 at T1462 *in vitro*, and RHEB overexpression rescues mTORC1 activity in cells. (A) An in-vitro kinase assay was performed using DYRK1A and kinase-dead DYRK1A (K188R) that were purified from bacteria. Flag-TSC2 and HA3-TSC1 were co-expressed in HEK293 cells and purified using a combination of (1:1) of HA and Flag beads. Beads were equilibrated with kinase assay buffer before the reactions were initiated on beads. After incubation for 30 min at 30°C, reactions were stopped by the addition of SDS loading buffer. Since bacterially purified DYRK1A is autophosphorylated, it exhibits a fuzzier signal, whereas kinase-dead DYRK1A is incapable of phosphorylation and appears as a sharp signal. (B-C) *RHEB* overexpression partially rescues the size of HEK293 cells. HEK293 cells were first transduced with shRNA lentivirus targeting DYRK1A or control and selected with 1 ug/ml Puromycin for three days, after which they were re-transduced with lentivirus expressing Flag-RHEB. The concentration of Puromycin was raised to 2ug/ml for the next 48 hours in order to select for the second round of transduction. (B) shows knockdown efficiency of DYRK1A and overexpression of RHEB. (C) Lower panel shows cell size analysis. Data represent the mean ± SD (n=3 biological replicates). Student's t-test was done to compare samples. Significant difference in p value = * ($p < 0.05$)

A

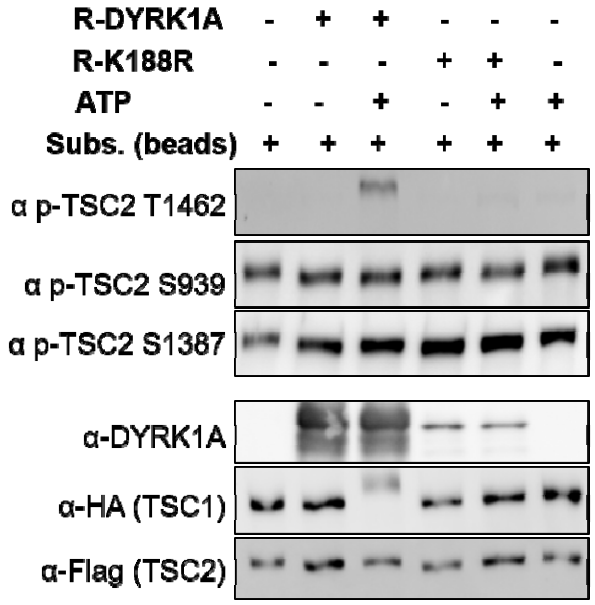
R-DYRK1A - + + - - -
R-K188R - - - + + -
ATP - - + - + +
Subs. (beads) + + + + + +
α p-TSC2 T1462
α p-TSC2 S939
α p-TSC2 S1387
α-DYRK1A
α-HA (TSC1)
α-Flag (TSC2)

B

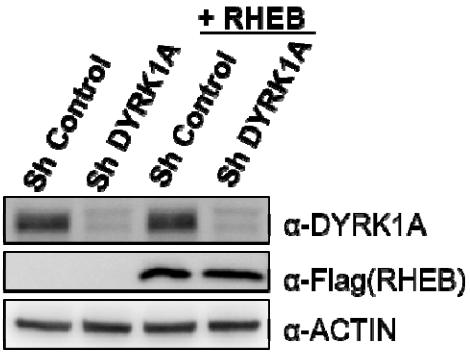
+ RHEB
Sh Control
Sh DYRK1A
Sh Control
Sh DYRK1A
α-DYRK1A
α-Flag(RHEB)
α-ACTIN

C

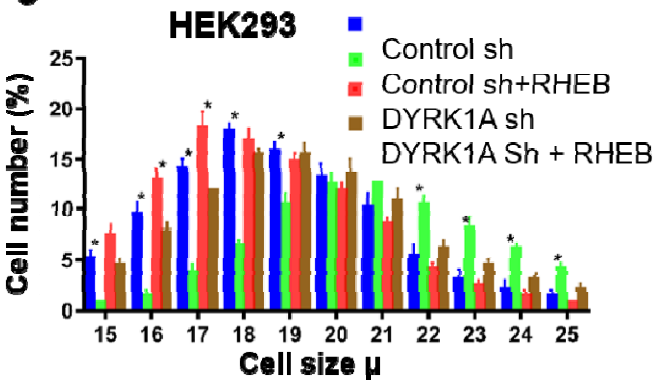
HEK293
Control sh
Control sh+RHEB
DYRK1A sh
DYRK1A Sh + RHEB
Cell number (%)
Cell size μ
0
5
10
15
20
25
15
16
17
18
19
20
21
22
23
24
25

Figure 5. *mnb* mutant phenotype can be rescued by TOR activation in flies. (A-F and J-L) 3rd instar larval NMJ (muscles 6/7) were stained using anti-HRP (Green) and anti-Dlg (Red). Muscles are stained with phalloidin (Blue, **A-F**). HRP (green) stains the entire neuron and Dlg (red) stains only boutons (Red+Green). **(G-I, M)** Quantification of bouton numbers, normalized to muscle area (Bouton-NMA). Error bars represent standard deviation. Statistical significance (*p*-values: *** < 0.001; ** < 0.01; * < 0.05) is calculated by unpaired student's t-test. **(A, B, G)** mnb^1 alleles show fewer boutons numbers as compared to wild-type (WT, Canton S) control **(B)**. Data are quantified in **G**. **(C, D, H)** *mnb* overexpression (*D42-Gal4*>UAS-*mnb,* **D**) increases bouton numbers as compared with mCherry overexpression (*D42-Gal4*>UAS-mCherry, Control, C). D42-Gal4 is a motor-neuron specific driver. Data are quantified in H. **(E, F, I**) Rheb overexpression (*D42-Gal4*>UAS-Rheb, F) increases bouton numbers as compared with mCherry overexpression (*D42-Gal4*>UAS-mCherry, Control, **E**). Data are quantified in **I**. **(J-M)** *Rheb* overexpression in *mnb* mutant (mnb^1/Y *D42-Gal4*>UAS-Rheb, **L**) suppressed bouton phenotype as compared to *mnb* mutant (mnb^1/Y *D42-Gal4*/+, **K**). Wild type is heterozygous *D42-Gal4* (+/Y; D42-Gal4/+, J). Data is quantified in **M**.

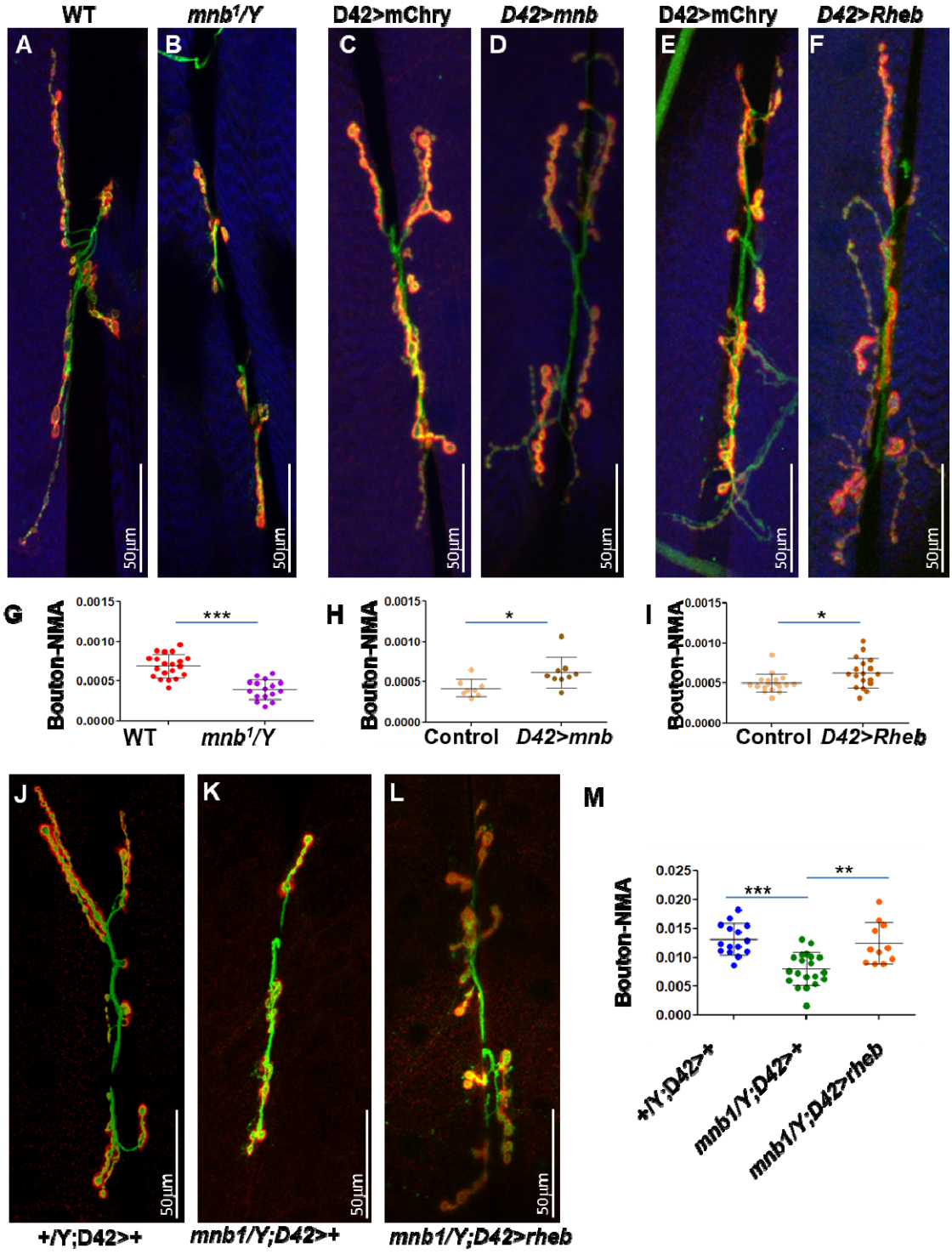
WT
mnb1/Y
D42>mChry
D42>mnb
D42>mChry
D42>Rheb
A
B
C
D
E
F
50µm
G
H
I
Bouton-NMA
0.0015
0.0010
0.0005
0.0000
***
*
WT
mnb1/Y
Control
D42>mnb
D42>Rheb
J
K
L
M
+/Y;D42>+
mnb1/Y;D42>+
mnb1/Y;D42>rheb
0.025
0.020
0.015
0.010
0.005
0.000
**

Methods

Expression plasmids and cell culture: pcDNA3 -HA3-TSC1 (Yue Xiong; Addgene #19911), pcDNA3 Flag TSC2 (Brendan Manning: Addgene #14129), LentiCRISPR v2 (Feng Zhang; Addgene #52961) plasmids were procured from Addgene. For expressing cDNA using lentivirus, LentiCRISPR v2 was modified by removing the U6 promoter and tracer RNA, and cDNA were cloned in place of SpCas9, and named LentiExp vector. *RHEB* sequence from pRK7-RHEB (John Blenis; Addgene #15888) was cloned into the LentiExp vector by replacing SpCas9. Expression was confirmed by western blot analysis. *DYRK1A* expression vector, *DYRK1A* shRNA, and control shRNA have been previously described (18). All constructs were confirmed by DNA sequencing. Expression of Flag-tagged proteins was induced with 250ng/ml Doxycycline for 36 to 48 h. HEK293, HEK293T and NIH3T3 cells were cultured in Dulbecco's Modified Eagle Medium (DMEM) supplemented with 10% Fetal Bovine Serum (FBS). All cell lines were obtained from the American Type Culture Collection (ATCC). Initially frozen stocks were tested for mycoplasma after thawing. Cell lines were maintained at 37°C under 5% CO_2.

Antibodies: Antibodies against Actin (AC026) and HA (AE008) were from Abclonal, anti-DDDDK from MBL (M185-3L), TSC1 (4906), TSC2 (4308), S6K (2708), pS6K (9205), S6 (2317), pS6 (4856) were from CST. DYRK1A antibody was generated in house and has been described before (18).

Cell extracts and Immunoblotting: For immunoblotting, total cell extracts were prepared. Briefly, collected cells were washed once with cold PBS and lysed in cold NP-40 lysis buffer (40mM HEPES, pH 7.4, 120mM NaCl, 1mM EDTA, 1% NP-40 [Igepal CA-630], 5% glycerol, 10 mM sodium pyrophosphate, 10 mM glycerol 2-phosphate, 50 mM NaF, 0.5 mM sodium orthovanadate and 1:100 protease inhibitors [Solarbio, P6730]) for 15 min on ice. Lysates were cleared by centrifugation, and protein concentration was measured using BCA kit. Western blot signals were quantified using ImageJ.

shRNA mediated knock down and overexpression of RHEB: Short hairpin RNA (shRNA) targeting *DYRK1A* have been previously described (18). Lentiviral particle preparation and infection were performed as previously described (18). Lentivirus-infected HEK293 and SH-

SY5Y cells were selected with 1 μg/mL(HEK293) or 2 μg/mL (SH-SY5Y) Puromycin respectively for four days.

For *RHEB* overexpression rescue of *DYKR1A* shRNA-mediated knockdown HEK293 cells, cells were first infected with lentivirus expressing shRNAs targeting control and *DYRK1A*, and then selected with 1μg/mL Puromycin for 48 hours. After selection cells were transduced with lentivirus expressing *Flag-RHEB*. These cells were further selected with 2μg/mL Puromycin for 48 hours before harvesting.

Serum starvation: shRNA treated HEK293 cells selected for 4 days with 1ug/ml puromycin were washed once with PBS and then DMEM without serum added. Serum starvation was performed for 12 hours. For stimulation with FBS (10%), pre-warmed FBS was directly added to the serum-free media for the time periods indicated.

CRISPR/Cas9 mediated *Dyrk1a* knockdown: NIH3T3 cells were transduced with lentiCRISPR v2 (Addgene plasmid #52961) containing either no sgRNA (control) or sgRNA targeting *Dyrk1a* (58). Transduced cells were selected with 3μg/mL Puromycin for 4 days before harvesting. sgRNA targeting mouse *Dyrk1a* is provided in supplemental table S1.

Cell size measurements: Cell size was measured and analyzed with a JIMBIO FIL electronic cell counter following the manufacturer's protocol. In short, 2.5×10^5 cells were seeded in 6-well plates. After 24 hours of culture, cells were trypsinized and taken up in full DMEM. Each cell line was measured three times; each measurement comprised three cycles of cell counts with intervals of 1 μm ranging from 4 to 30 μm. The sum of counts of viable cells in the range of 12 to 30 μm was plotted and quantified. Three biological replicates were performed per cell type (i.e., HEK293, SH-SY5Y and NIH3T3 cells [KD/KO and corresponding Control]). Control and corresponding KD/KO were compared with multiple unpaired t-tests. p values are presented as stars above the corresponding bar graphs; *, $p < 0.05$. HEK293 *Flag-DYRK1A* cell size was measured as above, except cells were induced with 40ng/mL Doxycycline for 48 hours.

Quantitative reverse transcription polymerase chain reaction (q-RT-PCR) assays: 2.5×10^5 cells were seeded in 6-well plates. After 48 hours of 40ng/mL Doxycycline induction, total RNA from fresh cells were extracted using RNA-easy Isolation Reagent (Vazyme) as per

the manufacturer's instructions. After determining the total RNA concentration and quality using a Nanodrop (Thermofisher), 1 μg RNA was used in 20 μL reaction mixture to reverse transcribe RNA using HiScript II 1st Strand cDNA Synthesis Kit (Vazyme R212) and stored at –20°C. 2μL was used to perform qPCR using ChamQ Universal SYBR qPCR Master Mix (Vazyme Q711) with 10 μM forward and reverse gene specific primers. The cycling consisted of 2 min at 95°C, followed by 40 cycles of 5 s at 95°C and 10 s at 60□. Following completion of the final cycle, a melting curve analysis was performed to monitor the purity of the PCR products. Each sample was analyzed in triplicate. Quantification was performed by means of the comparative Ct method ($2^{-\Delta\Delta CT}$). The mRNA expression of target genes was normalized to that of GAPDH, and the data are represented as the mean ± SEM of biological replicates.

Mass Spectrometry Analysis for identification of phosphorylated peptides of TSC1/TSC2:

Protein precipitation and digestion: Proteins were precipitated with TCA (trichloroacetic acid). The protein pellet was dried in Speedvac. The pellet was subsequently dissolved with 8 M urea in 100 mM Tris-Cl (pH 8.5). TCEP (final concentration is 5 mM; Thermo Scientific) and Iodoacetamide (final concentration is 10mM; Sigma) were added to the solution and incubated at room temperature for 20 and 15 minutes for reduction and alkylation respectively. The solution was diluted four times and digested with Trypsin at 1:50 (w/w; Promega).

LC/tandem MS (MS/MS) analysis of peptide: The peptide mixture was loaded on a home-made 15 cm-long pulled-tip analytical column (75 μm i.d.) packed with 3μm reverse-phase beads (Aqua C18, Phenomenex, Torrance, CA) connected to an Easy-nLC 1000 nano HPLC (Thermo Scientific, San Jose, CA) for mass spectrometry analysis. Data-dependent tandem mass spectrometry (MS/MS) analysis was performed with a Q Exactive Orbitrap mass spectrometer (Thermo Scientific, San Jose, CA). Peptides eluted from the LC system were directly electrosprayed into the mass spectrometer with a distal 1.8-kV spray voltage. One acquisition cycle includes one full-scan MS spectrum (m/z 300-1800) followed by top 20 MS/MS events, sequentially generated on the first to the twentieth most intense ions selected from the full MS spectrum at a 27% normalized collision energy. MS scan functions and LC solvent gradients were controlled by the Xcalibur data system (Thermo Scientific).

Data Analysis: The acquired MS/MS data were analyzed against a UniProtKB *Homo sapiens* database using Integrated Proteomics Pipeline (IP2, http://integratedproteomics.com/). In order to accurately estimate peptide probabilities and false discovery rates, we used a decoy database containing the reversed sequences of all the proteins appended to the target database. Carbamidomethylation (+57.02146) of cysteine was considered as a static modification and lysine phosphorylation (+79.9663) of STY as a variable modification.

Flag Immunoprecipitation: With detergent: 1×10^6 cells were seeded in 10 cm plates. After 24 hours of culture, cells were co-transfected with 5μg pcDNA-*Flag-DYRK1A*/deletion and 5μg *HA-TSC1* using PEI. After 48h, collected cells were washed once with cold PBS, and lysed in cold NP-40 lysis buffer (40mM HEPES, pH 7.4, 120mM NaCl, 1mM EDTA, 1% NP-40 [Igepal CA-630], 5% glycerol, 10 mM sodium pyrophosphate, 10 mM glycerol 2-phosphate, 50 mM NaF, 0.5 mM sodium orthovanadate and 1:100 protease inhibitors [Solarbio, P6730]) for 15 min on ice. Lysates were cleared by centrifugation, and protein concentration was measured using BCA kit. The supernatant was then incubated with Flag beads (Smart-Lifesciences, SA042005) for ~4 h at 4□. Finally, beads were washed with a lysis buffer without NP-40 three times and resuspended in a 1× SDS loading buffer. Samples were heated for 10 min at 95□ and separated by SDS-PAGE.

Overexpressed *DYRK1A* immunoprecipitation without detergent: Approximately 10^8 HEK293-*Flag-DYRK1A* (with 250ng/ml Doxycycline treatment), and parental cells were induced for 48h were collected and washed with PBS. Cells were swollen for 15 min in hypotonic buffer (Buffer A: 10 mM HEPES pH 7.9, 1.5 mM MgCl2, 10 mM KCl, 0.5 mM DTT supplemented with freshly prepared protease inhibitors, Solarbio, P6730). Swollen cells were dounced 20 times in a Wheaton Dounce homogenizer till about 90% of cells were lysed (as observed in a microscope). Lysates were then centrifuged at 5000-6000 g for 10 min at 4□. The supernatant was transferred to a new tube, and 0.11 volume of Buffer B (0.3M HEPES pH 7.9, 1.4M KCl, 0.03M $MgCl_2$) was added; the supernatant was then centrifuged at 12000g for 30 min. The supernatant was transferred to a new tube and incubated with Flag-beads (Smart-Lifesciences; SA042005) for ~4 h at 4□. Finally, beads were washed three times with wash buffer containing 150 mM NaCl and 0.2% Triton X-100 and resuspended in a 1× SDS loading buffer and analyzed by SDS-PAGE.

Endogenous *DYRK1A* immunoprecipitation without detergent: Approximately 10^8 HEK293 cells were swollen for 15 min in hypotonic buffer (Buffer A: 10 mM HEPES pH 7.9, 1.5 mM MgCl2, 10 mM KCl, 0.5 mM DTT supplemented with freshly prepared protease inhibitors, Solarbio, P6730). Swollen cells were dounced 20 times in a Wheaton Dounce homogenizer and centrifuged at 16000g for 30 min. Supernatant was transferred to a new tube, and 0.11 volume of Buffer B (0.3M HEPES pH 7.9, 1.4M KCl, 0.03M $MgCl_2$) was added and incubated with Protein A/G magnetic beads (Smart-Lifesciences, SM015001) for ~4 h at 4□. Finally, beads were washed three times with a wash buffer containing 150 mM NaCl and 0.2% Triton X-100 and resuspended in a 1× SDS loading buffer and analyzed by SDS-PAGE.

Kinase Assay: GST-DYRK1A and GST-DYRK1A K188R were cloned in pGEX-6p1vector, proteins were expressed in BL21 strain and purified using GST beads. FLAG-TSC2 and HA3-TSC1 were co-expressed in HEK293 cells, and Flag-Affinity purified. After wash, beads were rinsed with 1× kinase assay buffer (25 mM HEPES, pH 7.0, 5 mM MgCl2, 0.5 mM DTT), and kinase assay was performed on beads bound with FLAG-TSC2 and HA-TSC1. Equal amounts of GST-DYRK1A or GST-K188R were added to the Flag beads in presence/absence of ATP (100µM), and incubated at 30ºC for 30 min. Reactions were stopped by addition of 5× SDS loading dye and analyzed by SDS PAGE.

***Drosophila* culture:** Flies were grown in standard fly food at 25°C. Following genotypes were used in this study: Canton S (Bloomington Stock Center), *mnb[1]* (FBal0012364, (11), gift from Francisco J. Tejedor), UAS-*mnb* (FBtp0114512, (59), gift from Francisco J. Tejedor), UAS-*RHEB* (FBst0009688, Bloomington Stock Center), D42-Gal4 (FBti0002759, Bloomington Stock Center (49), P[(*45*)w[+mC]=UAS-Tor.TED]II (FBti0026636, (60), Bloomington Stock Center), UAS-mCherry (FBti0147460, Bloomington Stock Center).

***Drosophila* NMJ immunofluorescence staining and quantification:** For Immunofluorescence staining of NMJ the third instar larvae were fixed in 4% paraformaldehyde (Himedia Cat#TCL119) for 20 min at room temperature and washed in 1X PBST (0.2% Triton X-100). Antibodies were used at the following dilutions: Mouse anti-DLG 1:500 (DSHB 4F3, (59), Rabbit anti-HRP conjugated with alexa488 (dilution 1:500, Jackson 123-545-021), Goat anti-mouse conjugated with Alexa 555 (Dilution 1:500, Invitrogen A28180). Samples were imaged with a confocal microscope (Leica Stellaris 5 (PL APO 40X/1.30 oil objective) or Olympus FV3000 (UPLFLN 40X/1.30 oil objective). Images

were documented and quantified using ImageJ. We marked the HRP-labeled boutons to quantify NMJ phenotypes and manually counted the number. The number of boutons was then normalized to the muscle area (muscle 6/7), and the normalized data were compared between genotypes.

Statistical analysis. GraphPad Prism version 7.00 was used for statistical and statistical presentation of quantitation. *p* values are presented in the figures above or below the compared conditions. Two-way ANOVA followed by a Sidak's multiple comparisons test was applied to cell size data, p-S6 and p-S6k. Unpaired two-tailed Student's *t*-test was applied to DYRK1A protein expression. The data are represented as the mean ± SEM of three biological replicates.

Mass spectrometry dataset accessibility. Mass spectrometry data files for FLAG-DYRK1A affinity purifications and negative controls are available from Massive at /ftp://massive.ucsd.edu/MSV000085815/and ProteomeXchange (PXD020533). Original mass spectrometry data underlying this manuscript can be accessed after publication from the Stowers Original Data Repository at http://www.stowers.org/research/publications/libpb-1722.

Materials availability statement. Reagents created for this study are available from the authors upon request.

Supporting Information

Supporting Information is available online on elife website.

Acknowledgements

We thank Yue Xiong, Brendan Manning, Feng Zhang and John Blenis for plasmids and Francisco J. Tejedor for *mnb* fly strains. Liang Hu and Meng Huan Zhang for technical help in cloning. Fly strains obtained from the Bloomington Drosophila Stock Center (NIH P40OD018537) were used in this study.

Funding:

This work was supported in part by Yunnan High-end Foreign Experts program to MM, National Natural Science Foundation of China (31471206) to MM. Major Basic Research

Project of Science and Technology of Yunnan (202001BC070001) to LPBR. YZH, MPW and LF are supported by The Stowers Institute for Medical Research. MJ is supported by the Department of Atomic Energy (Project Identification No. RTI 4007), Department of Science and Technology, SERB (CRG/2020/003275), Department of Biotechnology (BT/PR32873/BRB/10/1850/2020), Government of India. MJ is a Ramalingaswami fellow, Department of Biotechnology, Government of India, under project number BT/RLF/Re-entry/06/2016. SNJ is supported by DBT/Wellcome trust India Alliance (grant no IA/I/18/1/503629) and intramural funding of CSIR-Centre for Cellular and Molecular Biology, Hyderabad, India.

References

1. Antonarakis SE. Down syndrome and the complexity of genome dosage imbalance. Nat Rev Genet. 2017;18(3):147-63.
2. Hammerle B, Ulin E, Guimera J, Becker W, Guillemot F, Tejedor FJ. Transient expression of Mnb/Dyrk1a couples cell cycle exit and differentiation of neuronal precursors by inducing p27KIP1 expression and suppressing NOTCH signaling. Development. 2011;138(12):2543-54.
3. Najas S, Arranz J, Lochhead PA, Ashford AL, Oxley D, Delabar JM, et al. DYRK1A-mediated Cyclin D1 Degradation in Neural Stem Cells Contributes to the Neurogenic Cortical Defects in Down Syndrome. EBioMedicine. 2015;2(2):120-34.
4. Malinge S, Bliss-Moreau M, Kirsammer G, Diebold L, Chlon T, Gurbuxani S, et al. Increased dosage of the chromosome 21 ortholog Dyrk1a promotes megakaryoblastic leukemia in a murine model of Down syndrome. J Clin Invest. 2012;122(3):948-62.
5. Courcet JB, Faivre L, Malzac P, Masurel-Paulet A, Lopez E, Callier P, et al. The DYRK1A gene is a cause of syndromic intellectual disability with severe microcephaly and epilepsy. J Med Genet. 2012;49(12):731-6.
6. Kay LJ, Smulders-Srinivasan TK, Soundararajan M. Understanding the Multifaceted Role of Human Down Syndrome Kinase DYRK1A. Adv Protein Chem Struct Biol. 2016;105:127-71.
7. Moller RS, Kubart S, Hoeltzenbein M, Heye B, Vogel I, Hansen CP, et al. Truncation of the Down syndrome candidate gene DYRK1A in two unrelated patients with microcephaly. Am J Hum Genet. 2008;82(5):1165-70.
8. Fotaki V, Dierssen M, Alcantara S, Martinez S, Marti E, Casas C, et al. Dyrk1A haploinsufficiency affects viability and causes developmental delay and abnormal brain morphology in mice. Mol Cell Biol. 2002;22(18):6636-47.
9. Fotaki V, Martinez De Lagran M, Estivill X, Arbones M, Dierssen M. Haploinsufficiency of Dyrk1A in mice leads to specific alterations in the development and regulation of motor activity. Behav Neurosci. 2004;118(4):815-21.
10. Degoutin JL, Milton CC, Yu E, Tipping M, Bosveld F, Yang L, et al. Riquiqui and minibrain are regulators of the hippo pathway downstream of Dachsous. Nat Cell Biol. 2013;15(10):1176-85.
11. Tejedor F, Zhu XR, Kaltenbach E, Ackermann A, Baumann A, Canal I, et al. minibrain: a new protein kinase family involved in postembryonic neurogenesis in Drosophila. Neuron. 1995;14(2):287-301.
12. Guedj F, Pereira PL, Najas S, Barallobre MJ, Chabert C, Souchet B, et al. DYRK1A: a master regulatory protein controlling brain growth. Neurobiol Dis. 2012;46(1):190-203.
13. Arbones ML, Thomazeau A, Nakano-Kobayashi A, Hagiwara M, Delabar JM. DYRK1A and cognition: A lifelong relationship. Pharmacol Ther. 2019;194:199-221.
14. Chen JY, Lin JR, Tsai FC, Meyer T. Dosage of Dyrk1a shifts cells within a p21-cyclin D1 signaling map to control the decision to enter the cell cycle. Mol Cell. 2013;52(1):87-100.
15. Recasens A, Humphrey SJ, Ellis M, Hoque M, Abbassi RH, Chen B, et al. Global phosphoproteomics reveals DYRK1A regulates CDK1 activity in glioblastoma cells. Cell Death Discov. 2021;7(1):81.
16. Pozo N, Zahonero C, Fernandez P, Linares JM, Ayuso A, Hagiwara M, et al. Inhibition of DYRK1A destabilizes EGFR and reduces EGFR-dependent glioblastoma growth. J Clin Invest. 2013;123(6):2475-87.
17. Di Vona C, Bezdan D, Islam AB, Salichs E, Lopez-Bigas N, Ossowski S, et al. Chromatin-wide profiling of DYRK1A reveals a role as a gene-specific RNA polymerase II CTD kinase. Mol Cell. 2015;57(3):506-20.

18. Li S, Xu C, Fu Y, Lei PJ, Yao Y, Yang W, et al. DYRK1A interacts with histone acetyl transferase p300 and CBP and localizes to enhancers. Nucleic Acids Res. 2018;46(21):11202-13.
19. Xue C, Gu X, Li G, Bao Z, Li L. Expression and Functional Roles of Eukaryotic Initiation Factor 4A Family Proteins in Human Cancers. Front Cell Dev Biol. 2021;9:711965.
20. Rehbein U, Prentzell MT, Cadena Sandoval M, Heberle AM, Henske EP, Opitz CA, et al. The TSC Complex-mTORC1 Axis: From Lysosomes to Stress Granules and Back. Front Cell Dev Biol. 2021;9:751892.
21. Ben-Sahra I, Manning BD. mTORC1 signaling and the metabolic control of cell growth. Curr Opin Cell Biol. 2017;45:72-82.
22. Saxton RA, Sabatini DM. mTOR Signaling in Growth, Metabolism, and Disease. Cell. 2017;169(2):361-71.
23. Dibble CC, Elis W, Menon S, Qin W, Klekota J, Asara JM, et al. TBC1D7 is a third subunit of the TSC1-TSC2 complex upstream of mTORC1. Mol Cell. 2012;47(4):535-46.
24. Li Y, Inoki K, Vacratsis P, Guan KL. The p38 and MK2 kinase cascade phosphorylates tuberin, the tuberous sclerosis 2 gene product, and enhances its interaction with 14-3-3. J Biol Chem. 2003;278(16):13663-71.
25. Tee AR, Anjum R, Blenis J. Inactivation of the tuberous sclerosis complex-1 and -2 gene products occurs by phosphoinositide 3-kinase/Akt-dependent and -independent phosphorylation of tuberin. J Biol Chem. 2003;278(39):37288-96.
26. Potter CJ, Pedraza LG, Xu T. Akt regulates growth by directly phosphorylating Tsc2. Nat Cell Biol. 2002;4(9):658-65.
27. Ma L, Chen Z, Erdjument-Bromage H, Tempst P, Pandolfi PP. Phosphorylation and functional inactivation of TSC2 by Erk implications for tuberous sclerosis and cancer pathogenesis. Cell. 2005;121(2):179-93.
28. Roux PP, Ballif BA, Anjum R, Gygi SP, Blenis J. Tumor-promoting phorbol esters and activated Ras inactivate the tuberous sclerosis tumor suppressor complex via p90 ribosomal S6 kinase. Proc Natl Acad Sci U S A. 2004;101(37):13489-94.
29. Corradetti MN, Inoki K, Bardeesy N, DePinho RA, Guan KL. Regulation of the TSC pathway by LKB1: evidence of a molecular link between tuberous sclerosis complex and Peutz-Jeghers syndrome. Genes Dev. 2004;18(13):1533-8.
30. Litovchick L, Florens LA, Swanson SK, Washburn MP, DeCaprio JA. DYRK1A protein kinase promotes quiescence and senescence through DREAM complex assembly. Genes Dev. 2011;25(8):801-13.
31. Soppa U, Schumacher J, Florencio Ortiz V, Pasqualon T, Tejedor FJ, Becker W. The Down syndrome-related protein kinase DYRK1A phosphorylates p27(Kip1) and Cyclin D1 and induces cell cycle exit and neuronal differentiation. Cell Cycle. 2014;13(13):2084-100.
32. Zhang P, Zhang Z, Fu Y, Zhang Y, Washburn MP, Florens L, et al. K63-linked ubiquitination of DYRK1A by TRAF2 alleviates Sprouty 2-mediated degradation of EGFR. Cell Death Dis. 2021;12(6):608.
33. Guard SE, Poss ZC, Ebmeier CC, Pagratis M, Simpson H, Taatjes DJ, et al. The nuclear interactome of DYRK1A reveals a functional role in DNA damage repair. Sci Rep. 2019;9(1):6539.
34. Li Y, Xie X, Jie Z, Zhu L, Yang JY, Ko CJ, et al. DYRK1a mediates BAFF-induced noncanonical NF-kappaB activation to promote autoimmunity and B-cell leukemogenesis. Blood. 2021;138(23):2360-71.
35. Menon VR, Ananthapadmanabhan V, Swanson S, Saini S, Sesay F, Yakovlev V, et al. DYRK1A regulates the recruitment of 53BP1 to the sites of DNA damage in part through interaction with RNF169. Cell Cycle. 2019;18(5):531-51.

36. Miyata Y, Nishida E. DYRK1A binds to an evolutionarily conserved WD40-repeat protein WDR68 and induces its nuclear translocation. Biochim Biophys Acta. 2011;1813(10):1728-39.
37. Sitz JH, Tigges M, Baumgartel K, Khaspekov LG, Lutz B. Dyrk1A potentiates steroid hormone-induced transcription via the chromatin remodeling factor Arip4. Mol Cell Biol. 2004;24(13):5821-34.
38. Astrinidis A, Cash TP, Hunter DS, Walker CL, Chernoff J, Henske EP. Tuberin, the tuberous sclerosis complex 2 tumor suppressor gene product, regulates Rho activation, cell adhesion and migration. Oncogene. 2002;21(55):8470-6.
39. Gao X, Pan D. TSC1 and TSC2 tumor suppressors antagonize insulin signaling in cell growth. Genes Dev. 2001;15(11):1383-92.
40. Tapon N, Ito N, Dickson BJ, Treisman JE, Hariharan IK. The Drosophila tuberous sclerosis complex gene homologs restrict cell growth and cell proliferation. Cell. 2001;105(3):345-55.
41. Inoki K, Zhu T, Guan KL. TSC2 mediates cellular energy response to control cell growth and survival. Cell. 2003;115(5):577-90.
42. Wu CW, Storey KB. mTOR Signaling in Metabolic Stress Adaptation. Biomolecules. 2021;11(5).
43. Manning BD, Tee AR, Logsdon MN, Blenis J, Cantley LC. Identification of the tuberous sclerosis complex-2 tumor suppressor gene product tuberin as a target of the phosphoinositide 3-kinase/akt pathway. Mol Cell. 2002;10(1):151-62.
44. Takahara T, Maeda T. Evolutionarily conserved regulation of TOR signalling. J Biochem. 2013;154(1):1-10.
45. Dimitroff B, Howe K, Watson A, Campion B, Lee HG, Zhao N, et al. Diet and energy-sensing inputs affect TorC1-mediated axon misrouting but not TorC2-directed synapse growth in a Drosophila model of tuberous sclerosis. PLoS One. 2012;7(2):e30722.
46. Natarajan R, Trivedi-Vyas D, Wairkar YP. Tuberous sclerosis complex regulates Drosophila neuromuscular junction growth via the TORC2/Akt pathway. Hum Mol Genet. 2013;22(10):2010-23.
47. Chen CK, Bregere C, Paluch J, Lu JF, Dickman DK, Chang KT. Activity-dependent facilitation of Synaptojanin and synaptic vesicle recycling by the Minibrain kinase. Nat Commun. 2014;5:4246.
48. Brand AH, Perrimon N. Targeted gene expression as a means of altering cell fates and generating dominant phenotypes. Development. 1993;118(2):401-15.
49. Gustafson K, Boulianne GL. Distinct expression patterns detected within individual tissues by the GAL4 enhancer trap technique. Genome. 1996;39(1):174-82.
50. Zhang HH, Huang J, Duvel K, Boback B, Wu S, Squillace RM, et al. Insulin stimulates adipogenesis through the Akt-TSC2-mTORC1 pathway. PLoS One. 2009;4(7):e6189.
51. Levy JA, LaFlamme CW, Tsaprailis G, Crynen G, Page DT. Dyrk1a Mutations Cause Undergrowth of Cortical Pyramidal Neurons via Dysregulated Growth Factor Signaling. Biol Psychiatry. 2021;90(5):295-306.
52. Kacsoh BZ, Barton S, Jiang Y, Zhou N, Mooney SD, Friedberg I, et al. New Drosophila Long-Term Memory Genes Revealed by Assessing Computational Function Prediction Methods. G3 (Bethesda). 2019;9(1):251-67.
53. Haas MA, Bell D, Slender A, Lana-Elola E, Watson-Scales S, Fisher EM, et al. Alterations to dendritic spine morphology, but not dendrite patterning, of cortical projection neurons in Tc1 and Ts1Rhr mouse models of Down syndrome. PLoS One. 2013;8(10):e78561.

54. Martinez de Lagran M, Benavides-Piccione R, Ballesteros-Yanez I, Calvo M, Morales M, Fillat C, et al. Dyrk1A influences neuronal morphogenesis through regulation of cytoskeletal dynamics in mammalian cortical neurons. Cereb Cortex. 2012;22(12):2867-77.
55. Park J, Chung KC. New Perspectives of Dyrk1A Role in Neurogenesis and Neuropathologic Features of Down Syndrome. Exp Neurobiol. 2013;22(4):244-8.
56. Barrada A, Djendli M, Desnos T, Mercier R, Robaglia C, Montane MH, et al. A TOR-YAK1 signaling axis controls cell cycle, meristem activity and plant growth in Arabidopsis. Development. 2019;146(3).
57. Zhang Y, Wen Z, Washburn MP, Florens L. Refinements to label free proteome quantitation: how to deal with peptides shared by multiple proteins. Anal Chem. 2010;82(6):2272-81.
58. Sanjana NE, Shalem O, Zhang F. Improved vectors and genome-wide libraries for CRISPR screening. Nat Methods. 2014;11(8):783-4.
59. Shaikh MN, Gutierrez-Avino F, Colonques J, Ceron J, Hammerle B, Tejedor FJ. Minibrain drives the Dacapo-dependent cell cycle exit of neurons in the Drosophila brain by promoting asense and prospero expression. Development. 2016;143(17):3195-205.
60. Hennig KM, Neufeld TP. Inhibition of cellular growth and proliferation by dTOR overexpression in Drosophila. Genesis. 2002;34(1-2):107-10.